Presented at the 24th European PV Solar Energy Conference and Exhibition, 21-25 September 2009, Hamburg, Germany

HIGH-EFFICIENCY N-TYPE SILICON SOLAR CELLS WITH FRONT SIDE BORON EMITTER

J. Benick[1], B. Hoex[2], G. Dingemanns[2], A. Richter[1], M. Hermle[1] and S. W. Glunz[1]
[1]Fraunhofer Institute for Solar Energy Systems (ISE), Heidenhofstrasse 2, D-79110 Freiburg, Germany
[2]Eindhoven University of Technology, P.O. Box 513, 5600 MB Eindhoven, The Netherlands
Phone +49-761-4588-5493; Fax +49-761-4588-9250; email: jan.benick@ise.fraunhofer.de

ABSTRACT: High-efficiency *n*-type PERL solar cells with a front side boron emitter passivated by ALD Al_2O_3 are presented within this work. For the applied PERL cell design two variations have been employed: i) different boron emitters (deep / shallow) and ii) different dielectric layers for rear side passivation (thermal grown SiO_2 and PECVD SiN_x). Both, thermal grown SiO_2 as well as PECVD SiN_x provide an effective passivation of the *n*-type rear surface with effective surface recombination velocities of 4 cm/s and 7 cm/s respectively. If the metalized rear side point contacts (with BSF) together with the recombination of the 1 Ω cm FZ base silicon are taken into account this results in saturation current densities of 30 fA/cm^2 and 37 fA/cm^2 respectively, limiting the open-circuit voltage (all recombination losses due to the front side are neglected) to 717 mV and 712 mV. The passivation of the boron emitter with ALD Al_2O_3 results in an emitter saturation current density as low as 11 fA/cm^2. Together with the losses at the rear side as well as the front side contacts this allows for an open-circuit voltage of the applied PERL solar cell design of ~700 mV. For *n*-type PERL solar cells featuring a lowly doped boron emitter as well as a SiO_2 passivated rear such a high open-circuit voltage (up to 703.6 mV) could be reached also at the device level, resulting in a conversion efficiency of 23.4%. Also for the PERL solar cells featuring a high surface concentration boron emitter with a PECVD SiN_x passivated rear, i.e. first steps towards an industrial structure, still a high conversion efficiency of 21.8% could be achieved. All cells have been shown to be perfectly stable under illumination at 1 sun.

Keywords: Silicon, *n*-type, High-Efficiency, Passivation,

1 INTRODUCTION

n-type silicon has an enormous potential for widescale applications in the photovoltaics industry. Its relative tolerance to common impurities (e.g. Fe) [1] potentially results in higher minority carrier diffusion lengths compared to *p*-type *c*-Si substrates with a similar impurity concentration. Furthermore *n*-type *c*-Si does not suffer from the boron-oxygen related light-induced degradation (LID), which is known to cause the light-induced degradation for *c*-Si solar cells based on *p*-type Cz *c*-Si [2].

In the following a short review of different solar cell structures that have been realized on *n*-type silicon will be given. The cell structures will be separated by the side where the *pn*-junction is placed, i.e. if the cells are front or rear side collecting.

1.1 Rear side collecting *n*-type solar cells

Rear side collecting solar cells always have stringent requirements on the silicon wafer quality, i.e. this type of solar cells mainly is restricted to monocrystalline silicon.

The p^+ emitter of rear side collecting solar cells mostly is realized by two methods, i.e. boron diffusion or aluminium alloying. For the former Zhao *et al.* reported efficiencies of 22.7% and 20.8% for passivated emitter with rear totally diffused (re-PERT) solar cells on 1.5 Ω cm FZ and 5 Ω cm Cz silicon respectively [3]. An efficiency of 22.0% was reported for solar cells that have a rear interdigitated contact scheme that is metallized by a single evaporation (RISE) on 1.5 Ω cm FZ silicon with a designated area of 4 cm^2 [4]. For laser grooved interdigitated backside buried contact (IBBC) solar cells Guo *et al.* presented efficiencies of 19.2% on 1 Ω cm FZ and 16.8% on Cz silicon [5]. For large area screen printed *n*-type Cz silicon solar cells Froitzheim *et al.* obtained an efficiency of 17.4% [6]. For the back junction back contact (BJBC) solar cell transferred into industrial production by Sunpower an average efficiency of 22.4% was reported for industrial production [7]. The highest confirmed efficiency for this cell structure are 22.7% [8].

For *n*-type solar cells featuring an aluminium alloyed rear side emitter Glunz *et al.* reported an efficiency of 19.4% for a laser fired local Al emitter (LFE) on 100 Ω cm FZ silicon. Results for *n*-type solar cells featuring a screen printed Al-p^+ back junction are presented by various authors [9-12]. Schmiga *et al.* reported an efficiency of 19% for cells with an unpassivated rear and 20.1% for cells where the rear side Al-p^+ emitter was passivated by Al_2O_3/SiO_x [13].

1.2 Front side collecting *n*-type solar cells

Solar cells featuring the *pn*-junction at the front side are not as restricted concerning the quality of the base silicon. Thus for these types of solar cells the utilization of *n*-type multicrystalline silicon might be a promising option.

For the heterojunction with intrinsic thin layer (HIT) solar cells that have been transferred into industrial production by Sanyo, an efficiency >20% is reported in mass production [14]. Recently an efficiency of 23.0% for this cell type was presented [15]. Boron doped front side emitters so far have been realized by epitaxial growth as well as by boron diffusion. For *n*-type solar cells with epitaxial emitters an efficiency of 16.3% has been reported by Schmich *et al.* [16]. For passivated emitter with rear totally diffused (PERT) solar cells with a diffused boron emitter Zhao *et al.* reported an efficiency of 21.9% on 0.9 Ω cm FZ silicon [17]. Unfortunately this solar cells passivated by a thermal SiO_2 have been shown not to be stable [18]. For passivated emitter with rear locally diffused (PERL) solar cells with an Al_2O_3 passivated front side boron

emitter Benick *et al.* reported an efficiency of 23.2% on 1 Ω cm FZ silicon [19]. Mihailetchi *et al.* reported an efficiency of 18.3% for a large area (156 cm^2) screen printed Cz (1.5 Ω cm) solar cell with the front side boron emitter passivated by a wet chemical grown ultrathin SiO_2 coated with PECVD SiN_x [20].

1.3 Dielectric layers for boron emitter passivation

SiO_2, the most effective passivation for highly doped *n*-type surfaces [21], does not show the same performance on highly boron-doped surfaces [18, 22-24]. The high boron solubility [25] combined with the presence of a small fixed positive charge density [26] contribute to this gap in performance. The second standard passivation layer for n^+-doped surfaces a-SiN_x:H does not passivate highly doped *p*-type surfaces effectively due to the high concentration of build-in *positive* charges [24, 27, 28]. Nevertheless, Chen *et al.* have shown a-SiN_x:H passivation on highly doped *p*-type surfaces with J_{0e} values below 10 fA/cm^2 for sheet resistivities above 100 Ω/sq [29]. However, no *n*-type cells have been fabricated using this approach which would demonstrate the potential of this technology on device level. Alternative passivation layers that are under investigation for passivation of highly doped *p*-type surface are a-Si:H and a-SiC_x:H. With a-Si:H J_{0e} values below 30 fA/cm^2 have been reached for sheet resistivities above 100 Ω/sq [24, 30]. a-SiC_x:H shows only poor passivation quality so far with $J_{0e} > 400$ fA/cm^2 on highly doped *p*-type surfaces ($R_{sheet} = 100$ Ω/sq) [31]. Apart from SiO_2 all other layers, especially if rich in Si, show a considerable absorption for photons with a wavelength <600 nm which is undesirable for the application as antireflection coating.

For passivation of highly doped *p*-type *c*-Si a dielectric containing a fixed *negative* charge density without any absorption in the visible part of the solar spectrum would be ideal. One dielectric layer meeting these specifications, which can be fabricated in a low temperature process is the negative-charge dielectric Al_2O_3. Hoex *et al.* measured emitter saturation currents below 10 fA/cm^2 on highly doped *p*-type *c*-Si surfaces of unmetalized lifetime samples coated with Al_2O_3 synthesized by atomic layer deposition (ALD) [32]. The high density of fixed negative charges (up to ~10^{13} cm^{-2}) within those layers provides an effective field effect passivation on highly *p*-type doped surfaces [33]. Due to the low deposition rate of the ALD technique also other technologies for the deposition of the Al_2O_3 are under investigation. Recently for Al_2O_3 deposited by PECVD [34, 35] and rf sputtering [36] an effective passivation of the surface was reported.

1.4 This work

In this work the focus is on the development of high-efficiency *n*-type PERL solar cells with the diffused front side boron emitter passivated by ALD Al_2O_3. Two variations of the PERL cells will be applied: i) different boron emitters (low / high surface concentration) and ii) different dielectric layers for the passivation of the rear side (thermal grown SiO_2 and PECVD SiN_x). In addition to the processed solar cells also the passivation quality of the front and rear side will be investigated on special lifetime test samples.

2 PASSIVATION OF N-TYPE REAR SIDE

2.1 Experimental

To investigate the passivation quality of thermal grown SiO_2 as well as PECVD SiN_x as the rear side passivation layer of *n*-type PERL solar cells symmetrical lifetime structures on 1 Ω cm *n*-type FZ silicon have been processed. After RCA clean the samples were either passivated by a 105 nm thick thermal grown SiO_2 (1050°C) or by a 80 nm thick PECVD SiN_x. After being coated with the passivation layer 2 µm of aluminium were evaporated on both sides of the samples and the samples achieved a forming gas anneal at 425°C. After this so called alneal step the aluminium was removed in HCL. The samples were characterized using the Quasi Steady State PhotoConductance (QSSPC) method. From these lifetime (τ_{eff}) measurements, the effective surface recombination velocity S_{eff} at $\Delta n = 10^{15}$ cm^{-3} has been determined according to

$$\frac{1}{\tau_{eff}} = \frac{1}{\tau_{bulk}} + \frac{2 \cdot S}{W}.$$

2.2 Results

The measured effective carrier lifetimes and the respective surface recombination velocities are summarized in Table I. The low surface recombination velocities of <7 cm/s for both dielectric layers prove the very effective passivation of the alnealed thermal SiO_2 as well as of the PECVD SiN_x.

Table I Effective lifetime and S_{pass} for the *n*-type rear side passivation with thermal grown SiO_2 and PECVD SiN_x.

	τ_{eff} [µs]	S_{pass} [cm/s]
Thermal SiO_2	1910	3.8
PECVD SiN_x ($n \approx 2.7$)	1307	6.8

However, to estimate the impact of the rear side on the solar cell also the metallized parts of the rear side have to be taken into account. Assuming ideal diode characteristics the open-circuit voltage of a solar cell can be calculated using the one-diode equation

$$V_{oc} = \frac{kT}{q} \ln\left(\frac{J_L}{J_{0e} + J_{0b}} + 1\right).$$

Herewith, J_{0b} the saturation current density of the base summarizes all contributions to the saturation current density originating from the rear side as well as from the base material of the solar cell. J_{0b} can be expressed by

$$J_{0b} = \frac{q n_i^2 D_p}{L N_D} \cdot \frac{S_{rear,eff} \cosh(W/L) + D_p / L \sinh(W/L)}{D_p / L \cosh(W/L) + S_{rear,eff} \sinh(W/L)}$$

Fischer [37] introduced an analytical model for the calculation of an effective surface recombination velocity of the point contacted solar cell rear side:

$$S_{rear,eff} = \frac{D_p}{W}\left[\frac{p}{2W\sqrt{\pi f}}\arctan\left(\frac{2W}{p}\sqrt{\frac{\pi}{f}}\right) - \exp\left(-\frac{W}{p}\right) + \frac{D_p}{fWS_{cont}}\right]^{-1} + \frac{S_{pass}}{1-f}.$$

$S_{rear,eff}$ denotes the effective SRV of the rear side, S_{cont} the SRV beneath the metal contacts, S_{pass} the SRV beneath the passivated area, f the metallization fraction, p the contact pitch and W the sample thickness. This model accounts for two regions with a difference in the surface recombination velocity, i.e. the area underneath the contacts (S_{cont}) and the passivated region in between (S_{pass}). In the case of the PERL cell design (see Fig. 4) with a highly doped BSF underneath the contacts there is a third region, a thin boundary strip around the contacts, which features the BSF diffusion but has a passivated surface ($S_{BSF,}$). To account for these two regions an average surface recombination velocity has to be applied for the S_{cont} parameter in the latter equation. In a good approximation the effective recombination velocity of the BSF can be calculated by the area weighted sum of the passivated and metallized fraction.

$$S_{cont,eff} = f_{metall}S_{metall,eff}f + (1-f_{metall})S_{BSF,eff}$$

For the applied BSF (3×10^{19} cm^{-3} surface concentration) $S_{metall,eff}$ results in ~90 cm/s and $S_{BSF,eff}$ for both dielectric layers can be determined to be ~40 cm/s. Thus, for the applied solar cells with a f_{met}/f_{BSF} faction of ~11% the $S_{cont,eff}$ can be determined to be ~45 cm/s. To calculate the effective surface velocity of the rear $S_{rear,eff}$ and the saturation current density of the bulk J_{0b}, a typical high efficiency rear side structure was assumed. The parameters are in detail: the contact pitch p = 250 µm, the BSF fraction f_{BSF} = 1.7% and the metallization fraction f_{met} = 0.2%. The resulting $S_{rear,eff}$ as well as the J_{0b} for the respective dielectric layers are summarized in Table II.

Table II Effective rear side recombination velocity and saturation current density of the bulk for the applied PERL solar cell structure passivated with thermal grown SiO_2 and PECVD SiN_x.

	$S_{rear,eff}$ [cm/s]	J_{0b} [fA/cm^2]
Thermal SiO_2	4.8	30
PECVD SiN_x ($n \approx 2.7$)	7.6	37

Thus the maximum open-circuit voltage of a solar cell (all other recombination losses due to the front side are neglected) can be determined to be ~717 mV for the rear side passivation with thermal SiO_2 and ~712 mV for the passivation with PECVD SiN_x.

3 BORON EMITTER PASSIVATION

2.1 Experimental

To investigate the passivation quality of the Al_2O_3 coating on highly boron diffused surfaces, symmetrical p^+np^+ lifetime samples on 10 Ω cm n-type silicon have been processed. Two different diffusion profiles have been applied. The first one corresponds to a more industrial type of emitter with a high surface doping (8×10^{19} cm^{-3}) and a relatively shallow profile (~0.4 µm). This emitter was diffused by a BBr_3 diffusion at 890°C (1 h). The second boron emitter corresponds to the optimum emitter shape to reach highest conversion efficiencies, i.e. low surface doping (6×10^{18} cm^{-3}), deep profile (1.5 µm). For this emitter the BSG (boron silicate glass) of the emitter diffused at 890°C was removed in HF (50%) and the wafers achieved a drive-in diffusion in Ar atmosphere followed by an oxidation at 1050°C. The corresponding profiles of both emitters are shown in Fig. 1.

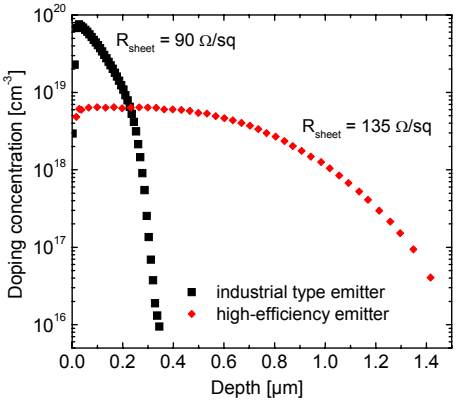

Fig. 1 Boron diffusion profiles of the industrial type as well as the high-efficiency type emitter.

Prior to the deposition of the Al_2O_3 passivation layer the samples were cleaned by a HNO_3 etch followed by a final dip in diluted HF (1%). The Al_2O_3 surface passivation layer then was deposited by plasma-assisted ALD at a temperature of 200°C. After being symmetrically coated with Al_2O_3 a part of the samples was quartered and the samples received a forming gas anneal at different temperatures. The samples were characterized using the Quasi Steady State PhotoConductance (QSSPC) as well as the Photo Luminescence (PL) method. Compared to the QSSPC the PL measurement is able to cover a broader range of the excess carrier density. From the measured effective lifetime in high level injection the emitter saturation current density was extracted according to [38]

$$\frac{1}{\tau_{eff}} - \frac{1}{\tau_{Auger}} = \frac{1}{\tau_{bulk,SRH}} + \frac{2\cdot J_{0e}}{qn_i^2W}\Delta n.$$

2.2 Al_2O_3 single layer

Fig. 2a) shows the injection level dependent lifetime (PL measurement) of several Al_2O_3 passivated emitter diffused samples after a forming gas anneal at 425°C. The samples feature different emitters (industrial type and high-efficiency) and the high-efficiency emitter samples also are coated by Al_2O_3 layers of different thicknesses (10 nm and 30 nm). In Fig. 2b) the $1/\tau_{eff}$-$1/\tau_{auger}$ versus Δn is plotted, to extract the emitter saturation current density. As can be seen an ideal linear relation between inverse lifetime and excess carrier density can be observed, allowing for a very accurate determination of J_{0e}. The extracted emitter saturation

current density of the samples annealed at different temperatures is shown in Fig. 3.

In the initial state, i.e. prior to the annealing step, no passivation is provided by the Al_2O_3. This can be related to the fact that a thermal activation is necessary to induce the negative charges at the interface. The optimum temperature for the annealing is around 450°C. A J_{0e} of approximately 40 fA/cm^2 was obtained for the sample with the industrial type boron emitter and between 20 to 25 fA/cm^2 for the samples with the high efficiency emitter. As expected the J_{0e} of the samples with the industrial emitter is above that measured for the high-efficiency emitter. The thickness of the Al_2O_3 coating though does not influence the quality of the passivation.

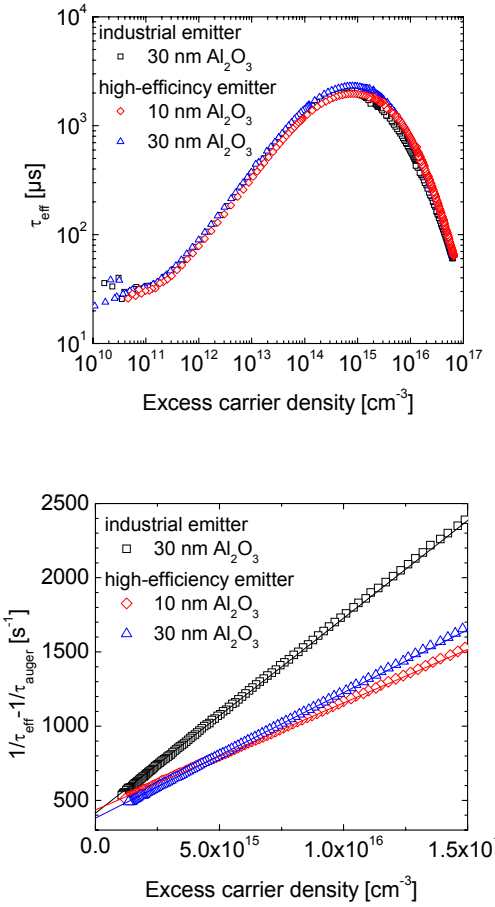

Fig. 2 Measured effective lifetime of the Al_2O_3 passivated boron diffused samples. All samples were annealed in forming gas at 425°C. a) shows the injection level dependent effective lifetime and in b) $1/\tau_{eff}$-$1/\tau_{auger}$ versus Δn is plotted to extract the emitter saturation current density.

However, a saturation current density in the range of ~10 fA/cm^2 is reported in literature for the Al_2O_3 passivation on high-efficiency like emitters [32]. The increased emitter saturation current density of the processed samples mainly can be related to the fact that these samples were quartered prior to the annealing. Due to the high base resistivity of the samples that is necessary to reach high-level injection during lifetime measurement the minority carrier diffusion length becomes very large (~10 mm). Thus, due to the exceptionally effective surface passivation of the samples with the high-efficiency emitter the non passivated edges of the samples have a detrimental influence of the measured lifetime. This is confirmed by the extracted saturation current density of samples that were not quartered prior to the annealing. On such a sample featuring a 20 nm thick Al_2O_3 coating a J_{0e} of 12.0 fA/cm^2 could be extracted.

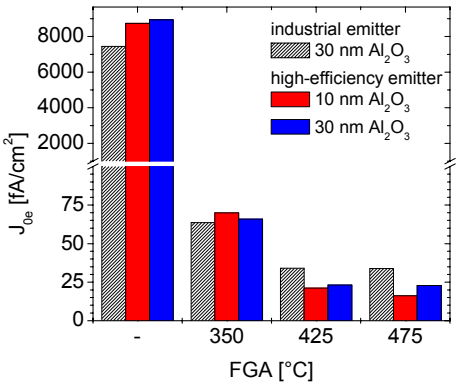

Fig. 3 Emitter saturation current density of the Al_2O_3 passivated boron diffused samples.

2.3 Ultrathin layers of Al_2O_3

To meet the high throughput demands of the photovoltaic industry with the relatively slow ALD technique (deposition rate ~1.5 nm/min) the Al_2O_3 surface passivation layer has to be as thin as possible.

Al_2O_3 layers with a thickness down to 1 nm were deposited on symmetrical lifetime samples featuring the high-efficiency type boron emitter (quartered wafers). The emitter saturation current density of those samples extracted from QSSPC measurements is shown in Fig. 4. For a thickness ≥10 nm a stable and effective surface passivation is provided by the Al_2O_3. For an Al_2O_3 thickness <10 nm the saturation current density increases. However, even for the 5 nm thick Al_2O_3 layer the surface still is effectively passivated as the J_{0e} is as low as ~40 fA/cm^2.

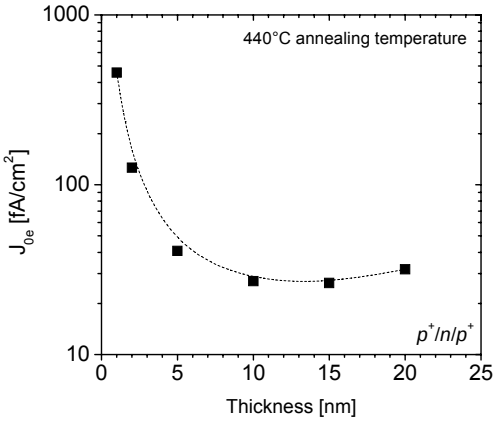

Fig. 4 Emitter saturation current density of the Al_2O_3 passivated boron diffused samples as a function of the Al_2O_3 thickness.

2.4 Al_2O_3/SiN_x layer stack

For the application at a solar cell the Al_2O_3 passivation layer will be combined with an additional antireflection coating, as the refractive index of the Al_2O_3 (1.65 @ 633 nm) is not within the optimum range for an antireflective coating. The antireflective coating most commonly applied in PV is PECVD SiN_x ($n \approx 2.0$ @ 633 nm). To investigate the influence of the SiN_x capping layer on the passivation quality of the Al_2O_3 passivation PECVD SiN_x was deposited on top of Al_2O_3 passivated boron diffused samples.

Table III shows the results for the extracted J_{0e} of a boron diffused sample passivated by a 20 nm thick Al_2O_3 with and without a SiN_x capping layer. For both samples the emitter saturation velocity is almost the same, 12 fA/cm^2 for the sample without SiN_x and ~11 fA/cm^2 for the sample additionally coated with the SiN_x antireflection coating. Thus it is evident that the passivation quality of the Al_2O_3 is not altered by the additionally coating with a PECVD SiN_x.

Table III Effective lifetime, J_{0e} and V_{oc} for boron diffused samples (high-efficiency emitter) passivated with an Al_2O_3/SiN_x stack.

	J_{0e} [fA/cm^2]
20 nm Al_2O_3	12.0
20 nm Al_2O_3 + 50 nm SiN_x	10.9
10 nm Al_2O_3 + 50 nm SiN_x	13.6

Table IV Emitter saturation current densities of the passivated and metallized as well as the area averaged of the respective parts. 30 fA/cm^2 and 37 fA/cm^2 have been applied for the J_{0b} for the calculation of the open-circuit voltage.

$J_{0e,cont}$	$J_{0e,cont} \times f_{cont}$	$J_{0e,pass}$	$J_{0e,pass} \times (1\text{-}f_{cont})$	J_{0e}	V_{oc}
		[fA/cm^2]			[mV]
High-efficiency emitter					
1800	18	10.9	10.8	28.8	700
Industrial emitter					
1600	16	35*	34.7	50.7	688
1600	16	64**	63.4	79.4	680

* FGA @ 350°C, ** FGA @ 425°C

Via the one-diode equation the open-circuit voltage of the final Al_2O_3 passivated solar cells can be estimated. To account for the front side contacts PC1D simulations have been performed to get an approximation for the emitter saturation current density underneath the contacted area ($S_{cont,front} = 10^6$ cm/s) and thus the $J_{0e,cont}$ can be calculated to be ~1800 fA/cm^2. With a metallization fraction of ~1% for the front side contacts the area weighted saturation current density of the J_{0e} can be calculated to

$$J_{0e} = f_{cont,front} \times J_{0e,cont} + (1 - f_{cont,front}) \times J_{0e,pass} .$$

Thus, together with the J_{0b} of 30 fA/cm^2 from section 2 the open-circuit voltage for the applied PERL solar cell structure (high efficiency emitter) that can be estimated from the lifetime samples is above 700 mV. A summary of the specific values for the respective parts of the J_{0e} is given in Table IV. From this it is evident that about >60% of the front side recombination is due to the contacted area.

4 SOLAR CELLS

3.1 Experimental

To investigate the excellent level of surface passivation of the Al_2O_3 coating on highly boron doped surfaces also at the solar cell level PERL solar cells were fabricated on ⟨100⟩ 1 Ω cm, FZ, *n*-type silicon wafers with a thickness of 250 µm. The processing of the Al_2O_3 passivated *n*-type PERL solar cells starts with the definition and the diffusion of the local phosphorus BSF at the rear side ($POCl_3$, 840°C, 1 h). After the removal of the PSG (phosphorus silicate glass) and the front side masking oxide a new oxide mask is grown and the front side texture by inverted pyramids is defined. To define seven cells on every wafer (area = 4 cm^2) emitter windows are opened in a new oxide mask and the boron emitter is diffused by a BBr_3 diffusion at 890°C (industrial type emitter, see Fig. 1). After the removal of the BSG (boron silicate glass) a part of the cells also achieved a drive-in diffusion in Ar atmosphere followed by an oxidation at 1050°C, resulting in a deeply driven-in boron emitter (high-efficiency emitter, see Fig. 1). This 105 nm thick SiO_2 also acts as the rear side passivation of those cells.

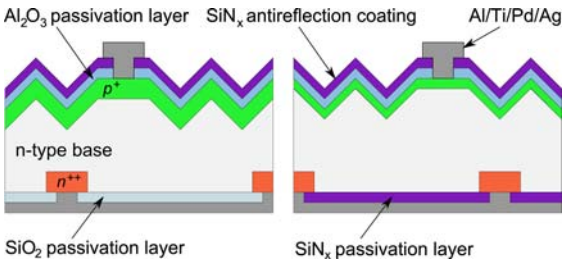

Fig. 5 PERL solar cell structure on *n*-type silicon. The surface is passivated by Al_2O_3.

The rear side of the industrial type solar cells was passivated by a PECVD SiN_x ($n \approx 2.7$). After the removal of the front side SiO_2 the boron emitter of all cells is passivated by a stack consisting of a 30 nm thick Al_2O_3 followed by a 40 nm thick SiN_x antireflection coating. The deposition of the Al_2O_3 was performed by plasma-assisted ALD (on an Oxford Instruments FlexAL^{TM} setup) at a temperature of 200°C at the TU/e Eindhoven. In a next step the rear side contacts were defined and realized by evaporation of 2 µm aluminium. To create the evaporated Al/Ti/Pd/Ag front side contacts the surface layers were structured by photolithography and wet chemically etched. To ensure the electrical contact and to remove the damage introduced by the x-rays during the e-gun evaporation processes the samples achieved an annealing step in forming gas ambient

(425°C for the cells with the high-efficiency emitter, 350°C for the cells with the industrial type emitter). In a last step the front side contacts were thickened by electroplated Ag. The final structure of these cells is shown in Fig. 5.

3.2 High-Efficiency solar cells

The one sun parameters of the *n*-type PERL solar cells featuring the high-efficiency front side boron emitter are summarized in Table V. Due to the effective front side passivation by the Al_2O_3 very high open-circuit voltages with an average of 696.9 mV for the processed 28 solar cells have been achieved. The best cell exhibits a V_{oc} of 703.6 mV, a J_{sc} of 41.5 mA/cm^2 and a *FF* of 80.2%, resulting in an independently confirmed solar cell efficiency of 23.4% (AM1.5G, Ed.2, 2008 [39]) (23.2% with AM1.5G, Ed.1, 1989 [40]). The exceptional high values for V_{oc}, despite the lack of a two-step emitter, prove the outstanding ability of Al_2O_3 for the passivation of highly doped *p*-type surfaces. The quantum efficiency of the best cell is shown in Fig. 6. Over a wide wavelength range (300 – 1000 nm) the internal quantum efficiency is 100%

Table V One-sun parameters of high-efficiency *n*-type PERL solar cells passivated by plasma enhanced ALD Al_2O_3. (AM1.5G (Ed.1), 100 mW/cm^2, 25°C, aperture area measurement).

	V_{oc} [mV]	J_{sc} [mA/cm^2]	*FF* [%]	η [%]
Average (28 cells)	696.9 ± 5.6	40.9 ± 0.3	78.8 ± 1.8	22.5 ± 0.7
Best	703.6	41.5	80.2	23.4*

* independently confirmed at Fraunhofer ISE CalLab

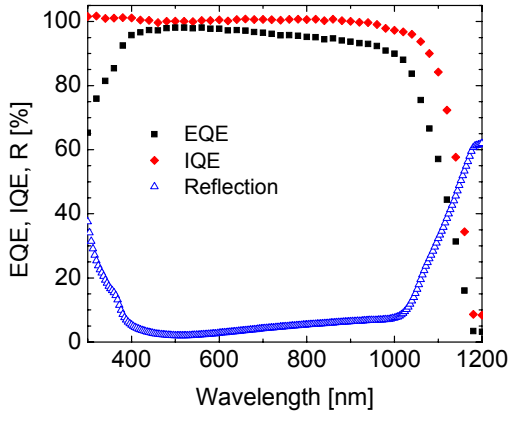

Fig. 6 IQE, EQE and reflection of the best Al_2O_3 passivated *n*-type PERL solar cell.

In total it can be said that also for solar cells with a front side boron emitter highest efficiencies can be reached, i.e. the boron emitter does not limit the solar cell efficiency.

3.2 First step towards an industrial structure

The results of the *I-V* measurement of the more industrial type *n*-type solar cells are shown in Table VI.

Despite the application of an industrial type emitter as well as the SiN_x passivation at the rear side, still an average conversion efficiency of well above 21% could be obtained. The cells still reach a high open-circuit voltage up to 676 mV. The difference in the open-circuit voltage of approximately 30 mV compared to the ~700 mV of the real high-efficiency solar cells is mainly related to the industrial type of emitter as well as to the fact that those cells were annealed only at 350°C (unfortunately these cells did not withstand a higher FGA temperature of 425°C). The SiN_x passivation at the rear side only increases the combined saturation current density of the bulk and the rear surface by 10 fA/cm^2 from ~30 fA/cm^2 to ~40 fA/cm^2. This increase in the saturation current density approximately accounts for a loss in the open-circuit voltage of ~5 mV. Again the measured V_{oc} is in good agreement to the V_{oc} extracted by the one-diode equation from the lifetime samples annealed at 350°C (see Table IV). As can also be seen in Table IV for a FGA temperature of 425°C an open-circuit voltage of ~690 mV should be within reach for this type of solar cells. The low FGA temperature also is the reason for the relatively poor *FF* that has been observed for these solar cells.

Table VI One-sun parameters of industrial type *n*-type PERL solar cells passivated by plasma enhanced ALD Al_2O_3 (AM1.5G (Ed.1), 100 mW/cm^2, 25°C, aperture area measurement).

	V_{oc} [mV]	J_{sc} [mA/cm^2]	*FF* [%]	η [%]
Average	673.6 ± 2.3	40.5 ± 0.1	78.1 ± 0.1	21.3 ± 0.4
Best	676.0	40.6	79.4	21.8

The IQE of the industrial type solar cells (see Fig. 7) also is 100% over a wide range (400 – 1000 nm). Only in the short wavelength range below 400 nm a slight decrease down to 95% can be observed.

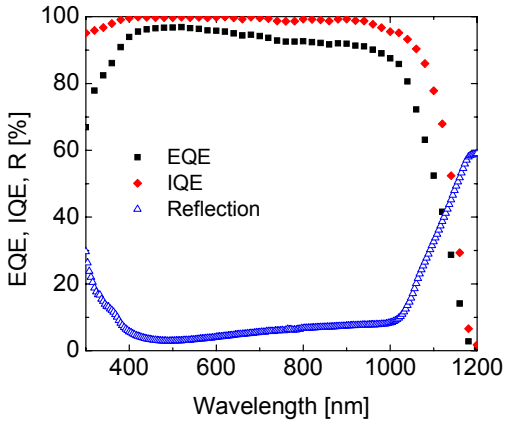

Fig. 7 IQE, EQE and reflection of the best Al_2O_3 passivated industrial type *n*-type PERL solar cell.

3.3 UV stability

To test for the UV stability of the Al_2O_3 passivated solar cells these cells were illuminated by a sun simulator up to

400 h. The degradation tests have been performed under different conditions. Some cells were covered by EVA and module glass to mimic the conditions of a PV module. Other cells only were covered by the module glass or are exposured directly to the irradiation of the sun simulator. The main effect of the EVA foil and the module glass with respect to the UV stability is the reduction of the UV fraction of the solar irradiance. All light with a wavelength below ~360 nm is cut-off by the EVA foil. The module glass shows a higher transparency in the UV range with a cut-off wavelength of 320 nm. For all other wavelength the transmittance of both, EVA and module glass, is above 90%.

The open-circuit voltage of the AL_2O_3 passivated *n*-type PERL solar cells as a function of the irradiation time is shown in Fig. 8. As the V_{oc} is very sensitive to the surface passivation this parameter is a good indicator for its degradation. As is evident from Fig. 7, the Al_2O_3 passivated solar cells are perfectly stable under one sun irradiation. The additional cover by EVA foil and/or module glass to reduce the UV fraction of the sun spectrum does not seem to improve the stability.

A perfect UV stability of Al_2O_3 on test structures already was reported by other authors. Hezel und Jaeger [41] reported an increase in the negative fixed charge density after irradiation with a Xenon lamp, improving the passivation via enhancement of the field effect by an increased accumulation. The D_{it} at the same time was reported not to be affected by the illumination. Also [42] reported a perfect UV stability of the Al_2O_3 passivation on highly boron doped surfaces.

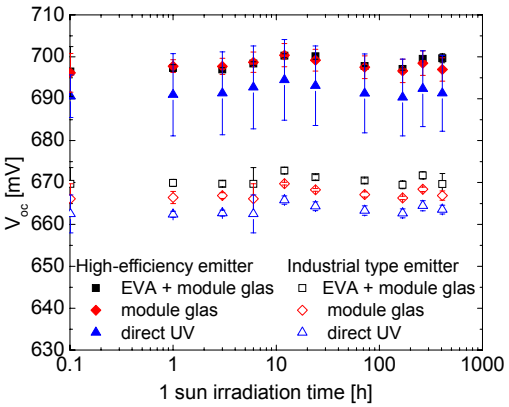

Fig. 8 Stability of the Al_2O_3 passivated *n*-type PERL solar cells under 1 sun irradiation.

5 CONCLUSIONS

For the applied *n*-type PERL solar cell structure a very high conversion efficiency of 23.4% and an open-circuit-voltage of 703.6 mV could be achieved. The extremely effective surface passivation of the *n*-type rear side (thermal grown SiO_2) as well as, in particular, of the boron doped emitter (ALD Al_2O_3) were the most important prerequisites for obtaining those high efficiencies. Also with the more industrial type solar cell featuring a high surface concentration boron emitter as well as a PECVD SiN_x passivated rear side still a high conversion efficiency of 21.8% could be reached. A more detailed analysis of the front as well as of the rear side passivation showed that the rear side together with the bulk silicon is responsible for a saturation current density of 30 fA/cm^2 in the case of the rear passivated with SiO_2 and 37 fA/cm^2 for the rear side passivated by PECVD SiN_x limiting the open-circuit voltage (all recombination losses due to the front side are neglected) to 717 mV and 712 mV. The passivation of the boron emitter with ALD Al_2O_3 results in an emitter saturation current density as low as 11 fA/cm^2. All cells have been shown to be perfectly stable under illumination at 1 sun.

6 ACKNOWLEDGEMENTS

The authors would like to thank S. Seitz, A. Leimenstoll and F. Schätzle for processing and T. Roth and E. Schäffer for measurements.

This work was funded by the German Federal Ministry for the Environment, Nature Conservation and Nuclear Safety under contract number 0329849A (Th-ETA).

7 REFERENCES

[1] D. Macdonald and L.J. Geerligs, Applied Physics Letters 85 (2004) 4061.

[2] S.W. Glunz, S. Rein, J.Y. Lee and W. Warta, Journal of Applied Physics 90 (2001) 2397.

[3] J. Zhao and A. Wang, Proceedings of the 4th World Conference on Photovoltaic Energy Conversion, Waikoloa, Hawaii, USA (2006) 996.

[4] P. Engelhart, N.-P. Harder, R. Grischke, A. Merkle, R. Meyer and R. Brendel, Progress in Photovoltaics: Research and Applications 15 (2006) 237.

[5] J.-H. Guo, B.S. Tjahjono and J.E. Cotter, Proceedings of the 31st IEEE Photovoltaic Specialists Conference, Orlando, USA (2005) 983.

[6] A. Froitzheim, K.A. Münzer, K.-H. Eisenrith, R. Tölle, R.E. Schlosser and M.G. Winstel, Proceedings of the 20th European Photovoltaic Solar Energy Conference, Barcelona, Spain (2005) 594.

[7] D. De Ceuster, P. Cousins, D. Rose, D. Vicente, P. Tipones and W. Mulligan, Proceedings of the 22nd European Photovoltaic Solar Energy Conference, Milan, Italy (2007) 816.

[8] P.J. Verlinden, R.A. Sinton, K. Wickham, R.A. Crane and R.M. Swanson, Proceedings of the 14th European Photovoltaic Solar Energy Conference, Barcelona, Spain (1997) 96.

[9] P. Hacke, J.D. Moschner, S. Yamanaka and D.L. Meier, Proceedings of the 19th European Photovoltaic Solar Energy Conference, Paris, France (2004) 1292.

[10] T. Buck, J. Libal, S. Eisert, R. Kopecek, K. Peter, P. Fath and K. Wambach, Proceedings of the 19th European Photovoltaic Solar Energy Conference, Paris, France (2004) 1255.

[11] R. Kopecek, T. Buck, J. Libal, I. Röver, K. Wambach, L.J. Geerligs, P. Sanches-Friera, J. Alonso, E. Wefringhaus and P. Fath, Proceedings of the 4th World Conference on Photovoltaic Energy Conversion, Waikoloa, Hawaii, USA (2006) 1044.

[12] V.D. Mihailetchi, D.S. Sainova, L.J. Geerligs and A. Weeber, Proceedings of the 22nd European Photovoltaic Conference, Milan, Italy (2007) 837.
[13] C. Schmiga, M. Hermle and S.W. Glunz Proceedings of the 23rd European Photovoltaic Solar Energy Conference, Valencia, Spain (2008).
[14] L. Korte, E. Conrad, H. Angermann, R. Stangl and M. Schmidt, Proceedings of the 22nd European Photovoltaic Solar Energy Conference, Milan, Italy (2007) 859.
[15] M.A. Green, K. Emery, Y. Hishikawa and W. Warta, Progress in Photovoltaics: Research and Applications 17 (2009) 320.
[16] E. Schmich, H. Lautenschlager and S. Reber, Technical Digest of the 17th International Photovoltaic Solar Energy Conference, Fukuoka, Japan (2007) 683.
[17] J. Zhao, A. Wang, P.P. Altermatt, M.A. Green, J.P. Rakotoniaina and O. Breitenstein, Proceedings of the 29th IEEE Photovoltaic Specialists Conference(2002) 218.
[18] J. Zhao, J. Schmidt, A. Wang, G. Zhang, B.S. Richards and M.A. Green, Proceedings of the 3rd World Conference on Photovoltaic Energy Conversion, Osaka, Japan (2003) 923.
[19] J. Benick, B. Hoex, M.C.M. van de Sanden, W.M.M. Kessels, O. Schultz and S.W. Glunz Applied Physics Letters 92 (2008) 253504/1.
[20] V.D. Mihailetchi, Y. Komatsu and L.J. Geerligs, Applied Physics Letters 92 (2008) 063510.
[21] J. Zhao, A. Wang, P.P. Altermatt, S.R. Wenham and M.A. Green, Proceedings of the 1st World Conference on Photovoltaic Energy Conversion, Hawaii, USA (1994) 87.
[22] R.R. King and R.M. Swanson, IEEE Transactions on Electron Devices 38 (1991) 1399.
[23] A. Cuevas, M. Stuckings, J. Lau and M. Petravic, Proceedings of the 14th European Photovoltaic Solar Energy Conference, Barcelona, Spain (1997) 2416.
[24] P.P. Altermatt, H. Plagwitz, R. Bock, J. Schmidt, R. Brendel, M.J. Kerr and A. Cuevas, Proceedings of the 21st European Photovoltaic Solar Energy Conference, Dresden, Germany (2006) 647.
[25] E.H. Nicollian and J.R. Brews, MOS Physics and Technology, Wiley, New York, 1982.
[26] S.W. Glunz, D. Biro, S. Rein and W. Warta, Journal of Applied Physics 86 (1999) 683.
[27] M.J. Kerr. Vol. PhD, pp. 228, Australian National University 2002.
[28] J. Libal, R. Petres, T. Buck, R. Kopecek, G. Hahn, R. Ferre, M. Vetter, I. Martín, K. Wambach, I. Roever, et al., Proceedings of the 20th European Photovoltaic Solar Energy Conference, Barcelona, Spain (2005) 793.
[29] F. Chen, I. Romijn, A. Weeber, J. Tan, B. Hallam and J. Cotter, Proceedings of the 22nd European Photovoltaic Solar Energy Conference, Milan, Italy (2007) 1053.
[30] H. Plagwitz, Y. Takahashi, B. Terheiden and R. Brendel, Proceedings of the 21st European Photovoltaic Solar Energy Conference, Dresden, Germany (2006) 688.
[31] M. Vetter, R. Ferre, I. Martín, P. Ortega, R. Alcubilla, R. Petres, J. Libal and R. Kopecek, Proceedings of the 4th World Conference on Photovoltaic Energy Conversion, Waikoloa, Hawaii, USA (2006) 1271.
[32] B. Hoex, J. Schmidt, R. Bock, P.P. Altermatt, M.C.M. van de Sanden and W.M.M. Kessels, Applied Physics Letters 91 (2007) 112107/1.
[33] B. Hoex, S.B.S. Heil, E. Langereis, M.C.M. van de Sanden and W.M.M. Kessels, Applied Physics Letters 89 (2006) 042112/1.
[34] S. Miyajima, J. Irikawa, A. Yamada and M. Konagai, Proceedings of the 23nd European Photovoltaic Solar Energy Conference, Valencia, Spain (2008) 1029.
[35] P. Saint-Cast, D. Kania, M. Hofmann, J. Benick, J. Rentsch and R. Preu, Applied Physics Letters (2009) accepted for publication
[36] T.-T. Li and A. Cuevas, Physica Status Solidi RRL 3 (2009) 160.
[37] B. Fischer. in Fachbereich Physik, pp. 198, Universität Konstanz, Konstanz 2003.
[38] D.E. Kane and R.M. Swanson, Proceedings of the 18th IEEE Photovoltaic Specialists Conference, Las Vegas, Nevada, USA (1985) 578.
[39] IEC. in International Standard IEC 60904-3 (IEC, ed.) 2008.
[40] IEC. in International Standard IEC 60904-3 (IEC, ed.) 1989.
[41] R. Hezel and K. Jaeger, Journal of the Electrochemical Society 136 (1989) 518.
[42] J. Schmidt, A. Merkle, R. Bock, P.P. Altermatt, A. Cuevas, N.-P. Harder, B. Hoex, M.C.M. van de Sanden, W.M.M. Kessels and R. Brendel, Proceedings of the 23rd European Photovoltaic Solar Energy Conference, Valencia, Spain (2008).